REPORT

Evidence for amorphous calcium carbonate originated mid-lithospheric discontinuities

Mingqiang Hou,[1,7] Ming Hao,[2,7] Jin Liu,[3,*] Xiaowan Su,[4] Wen-Yi Zhou,[5] Xiaoming Cui,[1] Rostislav Hrubiak,[6] Heping Sun,[1] and Jin Shelley Zhang[5,*]
*Correspondence: Jinzhang@tamu.edu (J. Z.); jinliu@ysu.edu.cn(J. L.)
Received: June 17, 2024; Accepted: October 10, 2024; Published Online: October 17, 2024; https://doi.org/10.59717/j.xinn-geo.2024.100098

GRAPHICAL ABSTRACT

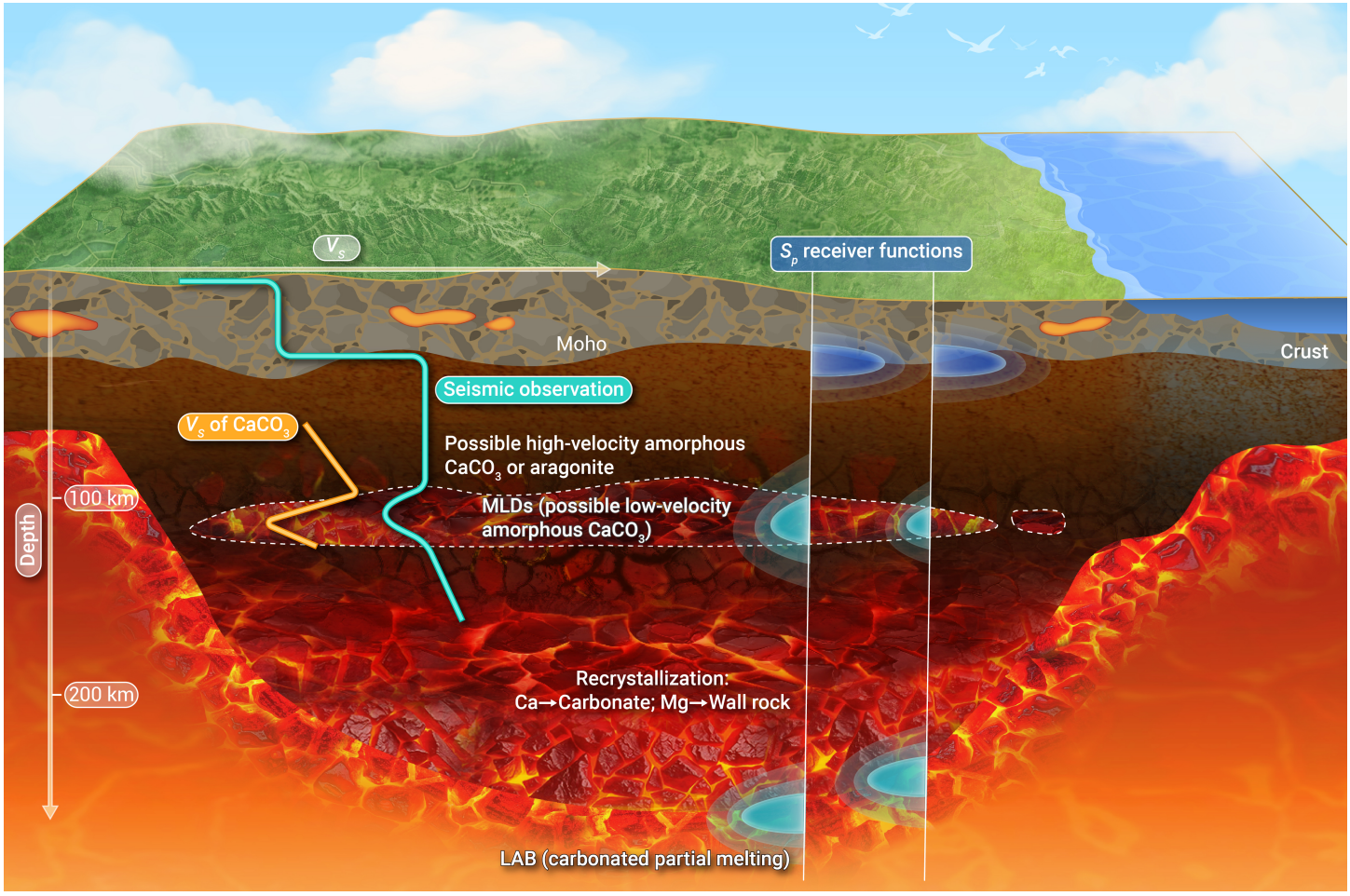

PUBLIC SUMMARY

- We measured the acoustic velocity of $CaCO_3$ under high-pressure and high-temperature conditions.
- Distinct velocity drops were observed in amorphous $CaCO_3$ around 3 GPa.
- The presence of 1–2 vol.% $CaCO_3$ in the craton would form the seismic mid-lithospheric discontinuities.

REPORT

Evidence for amorphous calcium carbonate originated mid-lithospheric discontinuities

Mingqiang Hou,[1,7] Ming Hao,[2,7] Jin Liu,[3,*] Xiaowan Su,[4] Wen-Yi Zhou,[5] Xiaoming Cui,[1] Rostislav Hrubiak,[6] Heping Sun,[1] and Jin Shelley Zhang[5,*]

[1]State Key Laboratory of Geodesy and Earth's Dynamics, Innovation Academy for Precision Measurement Science and Technology, CAS, Wuhan 430077, China
[2]Earth and Planets Laboratory, Carnegie Institution for Science, Washington 20015, USA
[3]Center for High Pressure Science, State Key Laboratory of Metastable Materials Science and Technology, Yanshan University, Qinhuangdao 066004, China
[4]State Key Laboratory of Earthquake Dynamics, Institute of Geology, China Earthquake Administration, Beijing 100029, China
[5]Department of Geology and Geophysics, Texas A & M University, College Station 77843, USA
[6]HPCAT, Advanced Phonon Source, Argonne National Laboratory, Argonne 60439, USA
[7]These authors contributed equally
*Correspondence: Jinzhang@tamu.edu (J. Z.); jinliu@ysu.edu.cn(J. L.)

Received: June 17, 2024; Accepted: October 10, 2024; Published Online: October 17, 2024; https://doi.org/10.59717/j.xinn-geo.2024.100098

Citation: Hou M., Hao M., Liu J., et al., (2024). Evidence for amorphous calcium carbonate originated mid-lithospheric discontinuities. The Innovation Geoscience **2(4)**: 100098.

The cratonic lithosphere is a vast host for deep recycled carbon, trapping up to several weight percent CO_2 at depths overlapping the seismic mid-lithospheric discontinuities (MLDs). However, the role of carbonates, especially for the latest discovered amorphous calcium carbonate ($CaCO_3$), is underestimated in the formation of MLDs. Using the pulse-echo-overlap method in a Paris-Edinburgh press coupled with synchrotron X-ray diffraction, we explored the acoustic velocities of $CaCO_3$ under high pressure-temperature (*P-T*) conditions relevant to the cratonic lithosphere. Two anomalous velocity drops were observed associated with the phase transition from aragonite to amorphous phase and with the pressure-induced velocity drop in the amorphous phase around 3 GPa, respectively. Both drops are comparable with approximately 35% and 52% reductions for compressional (V_P) and shear (V_S) wave velocities, respectively. The V_P and V_S values of the amorphous $CaCO_3$ above 3 GPa are about 1/2 and 1/3 of those of the major upper-mantle minerals, respectively. These velocity reductions caused by the presence of $CaCO_3$ would readily cause MLDs at depths of 70–120 km dependent on the geotherm even if only 1–2 vol.% $CaCO_3$ is present in the cratonic lithosphere.

INTRODUCTION

Cratons are the cores of tectonomagmatically quiescent continents for at least 2.5 Ga featured with multiple physicochemical peculiarities, amongst which MLDs are the most distinguished one besides cool geothermal gradient, strong Fe- and H_2O-depletions, and multiple metasomatisms.[1,2] The MLDs produce both positive and negative, but mostly negative, seismic velocity gradients at depths of 60–160 km in the cratonic lithospheres.[3–9] Although the depths of the majority of MLDs are slightly different, they are predominantly located at 70–120 km.[4,10] The 2–10% reduction in the V_S has been attributed to several attractive origins including partial melting, elastically accommodated grain boundary sliding (EAGBS), layered composition, layered anisotropy, and enrichment of seismically slow metasomatic minerals.[3–5] Recent studies indicate that partial melting and EAGBS are inadequate to account for the MLDs since the geotherms of most MLDs falls between approximately 1,000–1,200 K, which are well below the occurrence threshold (>1,300 K) of partial melting and EAGBS.[3,5,11] The observed wide depth ranges of MLDs suggest a non-mineral phase transition origin,[4] let alone the fact that no phase transition in the volumetrically dominated olivine and pyroxene occur at the relevant depth ranges in the upper mantle.[12] The presence of a composition or seismically anisotropic layer is insufficient to be a global genesis as well.[3,5]

Currently, the accumulation of seismically slow metasomatic minerals has attracted the most attentions.[3,11,13–15] Rader et al.[4] and Eeken et al.[11] pointed out that 5–10% hydrous minerals (e.g., amphibole and phlogopite) or 10–15% $CaCO_3$ aragonite could reproduce the observed seismic signatures of the MLDs. Notably, amphibole is stable below 3 GPa and 1,350 K[16] and the enrichment of amphibole can only explain the MLDs at depths shallower than 90 km. At depths greater than 90 km, phlogopite would be the main geological origin of the MLDs. $CaCO_3$ aragonite may work in the same way as these hydrous minerals.[4,11] However, the high *P-T* electrical conductivity of amphibole delimits the maximum fraction of hydrous minerals less than 1.5% to reconcile the magnetotelluric observations.[17,18] Another consequence of the enrichment of hydrous minerals in the MLDs is the young-age rocks sandwiched by old rocks, but the global resetting of the age in these regions has not been observed.[19] The enrichment of carbon in the lithosphere is feasible and has been estimated to be 0.43–0.86 wt%.[20] This corresponds to ~3–6 wt% carbonates in the MLDs, which is far below the necessary amount (10–15%) of aragonite. Intriguingly, aragonite-structured $CaCO_3$ enters the amorphous phase above 2 GPa and 1,000 K relevant to MLD conditions.[21] Such an amorphous phase transition generally causes a dramatic reduction in sound velocities, which potentially provides new insights into the origins of the MLDs.

MATERIALS AND METHODS

The starting material is reagent $CaCO_3$ powder (grain size: ~1 μm) purchased from Alfa Aesar Company with a purity of 99.99% (CAS No.: 471-34-1). The $CaCO_3$ powder was pre-compressed to a cylinder with 0.8 mm in height and 2 mm in diameter using a tungsten steel compressor. Then the sample cylinder was loaded into a standard high-pressure and high-temperature Paris-Edinburgh (PE) cell assembly (see Supplementary Information) and compressed above 2 GPa before measurement. The sample porosity should be extremely low due to the soft nature of the sample. Although Paris-Edinburgh press generates uniaxial stress, with the soft $CaCO_3$ sample sandwiched by hard Al_2O_3, hydrostatic compression is likely achieved during the experiments.

The experiments were conducted by using a VX-3 Paris-Edinburgh (PE) press at the High-Pressure Collaborative Access Team (HPCAT 16-BM-B) at the Advanced Photon Source, Argonne National Laboratory, USA. The schematic of the PE cell assembly is shown in Figure S1. The sample was placed between the Al_2O_3 buffer rod and the backing. An MgO ring surrounding the sample was used to calibrate the pressure. The pressure was determined by thermal equation of state of MgO which surrounds the sample (the white part inner the graphite heater in Figure S1). The 2θ angle is 15° for all the X-Ray diffraction measurements. Pre-calibrated power-temperature relations was calibrated in separated no-X-ray experiments and employed to determine the temperature.[22] The uncertainties of pressure and temperature are 0.5 GPa and 100 K, respectively.

The pulse-echo overlap technique was employed to obtain the ultrasonic V_P and V_S signals of the $CaCO_3$ sample. An ultrasonic excitation sine wave of 3-periods long, containing compressional and shear components, was generated using 10° Y-cut $LiNbO_3$ transducer. The wave was reflected at the buffer-rod/sample (R1) and sample/backing (R2) interfaces and the travel time (t) of the ultrasonic wave in the sample was determined by R1 and R2 signals. Electrical sine waves were generated by a waveform generator (Tektronix AFG3251) from 12 to 45 MHz with a step of 1 MHz. No overlapping between the R1 and R2 echoes has been observed in all the experimental runs. Ultrasonic signals with 30-45 MHz and 12-20 MHz are employed to obtain the travel time of V_P and V_S, respectively. The sample length (l) was measured by polychromatic X-ray radiography. Although significant deformation of the assembly could occur at high temperature, large volume expansion

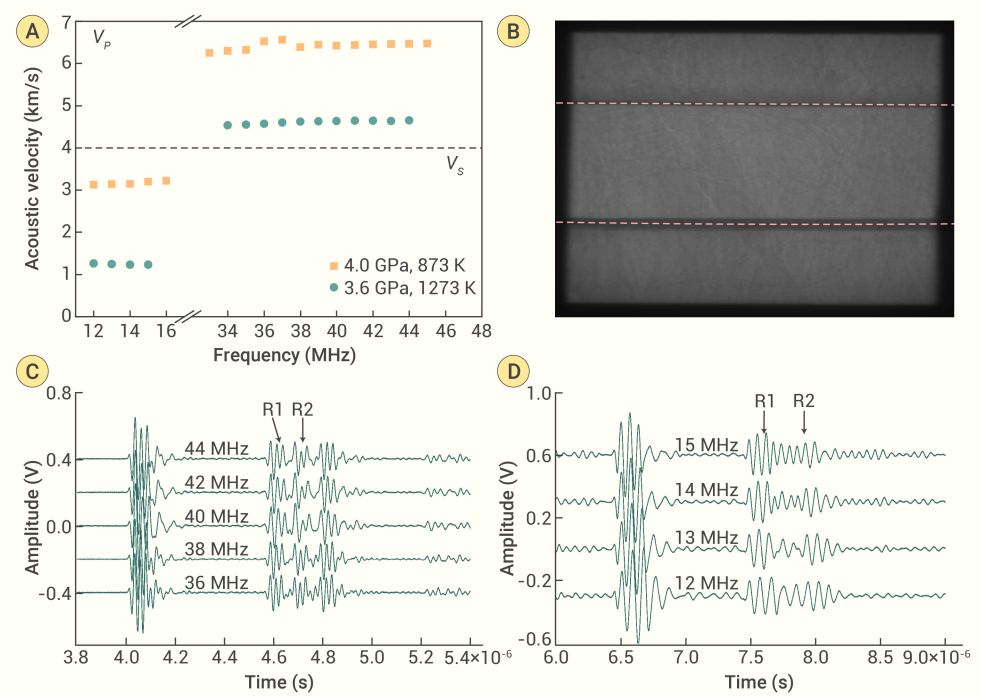

Figure 1. Acoustic velocity measurements of $CaCO_3$ at high pressure and temperature (A) Acoustic velocities as a function of frequency. Black squares: aragonite at 4.0GPa and 873K; blue circles: amorphous $CaCO_3$ at 3.6 GPa and 1,273K. The uncertainties of the measured acoustic velocities are less than 1.2% and the error bars are within the symbols. (B) Polychromatic X-ray radiograph. The red dashed lines denote the interfaces of the sample/buffering rod and sample/backing rod. The sample length (l) can be determined by the pixels between the two dashed lines in the image. (C) and (D): The V_P and V_S signals (R1 and R2) of $CaCO_3$ at 3.6 GPa and 1,273 K as a function of the acoustic frequency. 33–45 MHz and 12–16 MHz ultrasonic echoes are used to determine the time intervals of V_P and V_S, respectively.

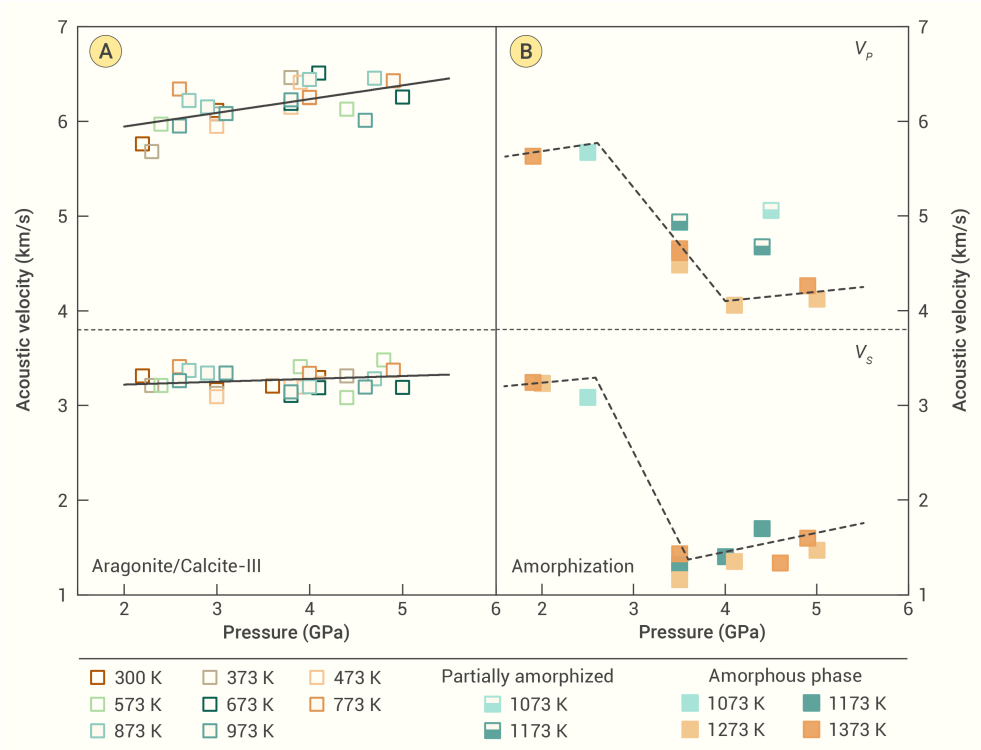

Figure 2. The acoustic velocities of aragonite/calcite (A) and amorphous $CaCO_3$ (B) at elevated pressures and temperatures The solid lines in (A) are linear fits to the experimental V_P and V_S values and the curves in (B) are drawn to guide eyes. The uncertainty of the pressure is 0.5 GPa at high temperature which is not plotted in the data for clarity. The error bars of the acoustic velocities are smaller than the symbols.

across the aragonite-amorphization phase transition would act as a tradeoff to avoid the overlap of the R_1 and R_2 signal. The travel time (t) of the elastic waves through the sample could be determined by R_1 and R_2. The sample length (l) was delimited by white X-ray radiography measurements. The acoustic velocity can be calculated by

$$V = \frac{2l}{t} \quad (1)$$

where V corresponds to the V_P or V_S, l is the thickness of the sample, and t is the travel time of ultrasonic signals determined by R_1 and R_2, respectively. The method in more details can be found in Kono et al.[22] When the Vp and Vs derived from the experimental data collected at different frequencies are identical, we consider these velocity measurements are reliable. The total uncertainties of the derived acoustic velocities are about 1.2% which originated from two aspects: (1) uncertainties in the sample length and travel time (t) of signal in the sample (less than 0.5%) and (2) frequency-induced uncertainty (0.7%).

RESULTS

In this study, we measured the acoustic velocities of aragonite and amorphous $CaCO_3$ at 2.0–5.5 GPa up to 1,373 K using the pulse-echo overlap technique in a Paris-Edinburgh press. The representative radiograph, ultrasonic signals, and acoustic velocities. as a function of frequency are presented in Figure 1. A wide range of frequencies from 12 to 45 MHz were scanned with a step of 1 MHz to obtain the travel time (t) of the longitudinal (V_P) and transverse (V_S) ultrasonic signals throughout the sample on the basis of their different frequency sensitivities. High-quality R1 and R2 waveforms (Figures 1C-D) were obtained to determine the t up to 1,373 K at high pressure. The acoustic velocities derived from varying frequencies agree with each other within the experimental uncertainties, indicating the reliability of the V_P and V_S values measured in this study.

The measured acoustic velocities of calcite, aragonite and amorphous $CaCO_3$ are shown in Figure 2. At 300–373 K and 3.0 (1)–4.5 (1) GPa, $CaCO_3$ is in the calcite-III phase[23] and its V_P and V_S values are about 6.2 and 3.2 km s^{-1}, respectively. They are in good agreement with previously published literature values.[24] At 473(100) K, the calcite-III transforms into aragonite.[21] The V_P and V_S values of aragonite are in the range of 6.00 (7) –6.51 (8) km s^{-1} and 3.08 (4) –3.48 (4) km s^{-1}, respectively, at 473–973 K and 3.0 (1)–5.0 (1) GPa. The pressure dependences of the V_P and V_S for aragonite are 0.14 (7) and 0.04 (3) km s^{-1} GPa^{-1}, respectively, whereas their temperature dependencies are fairly

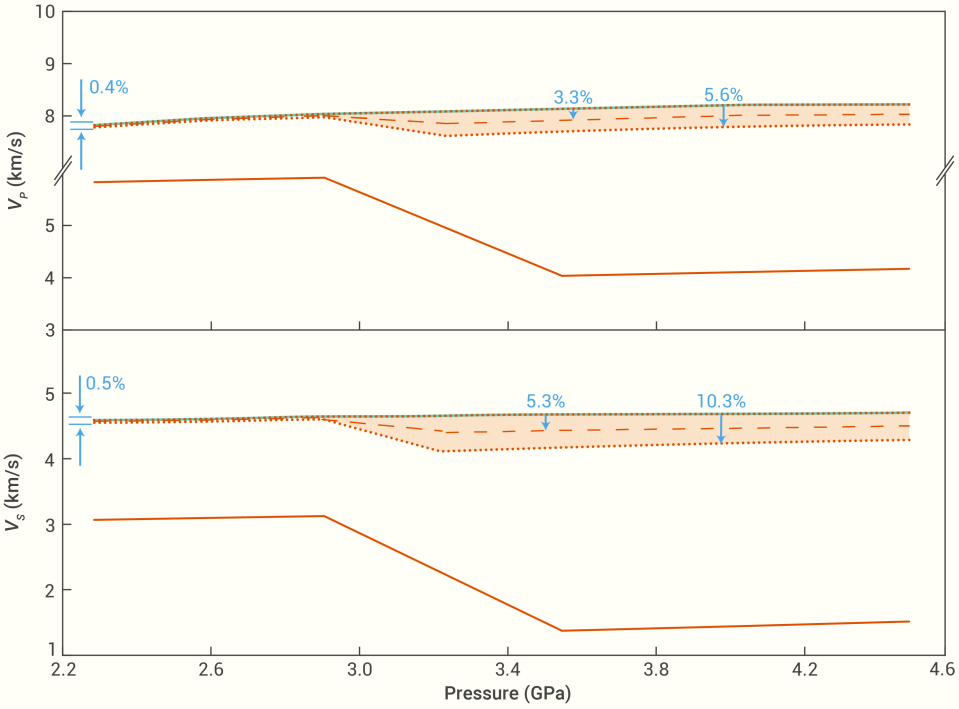

Figure 3. The seismic velocities of the pyrolite + 2 vol.% amorphous $CaCO_3$ along a typical craton geotherm with a surface heat flux of 40 mW/m² The solid black and blue curves represent the seismic velocities of pyrolite and amorphous $CaCO_3$, respectively. The shaded blue areas are bounded by the Voigt (up) and Reuss average of seismic velocities of pyrolite + 2 vol.% amorphous $CaCO_3$. The dashed curve is obtained using the Hill average. The red arrows denote the velocity reductions of the Reuss bound and Hill average compared with those for pure pyrolite.

small within the experimental uncertainties. It should be noted that no abrupt changes in the acoustic velocities are observed across the calcite-III to aragonite phase transition.

As the temperature was increased to greater than 1,000 K, the aragonite gradually transformed into an amorphous phase as reported previously.[21] This was clearly observed in the energy-dispersive X-ray diffraction (EDXRD) patterns of the $CaCO_3$ samples (Figure S2). The acoustic velocities of amorphous $CaCO_3$ exhibited two distinct characteristics. Below ~2.6 GPa, the V_P and V_S values of the amorphous phase and aragonite are comparable. That is, there were no obvious difference can be identified even if the data scattering is considered. As the pressure increases, both the V_P and V_S values of amorphous $CaCO_3$ gradually decrease within a narrow pressure range of ~1 GPa and then monotonically increase. The pressure-induced velocity reductions have been reported in amorphous SiO_2, $MgSiO_3$, (Fe, Al)-bearing silicate, and Icelandic basaltic glass at 2–5 GPa.[25-27] Such pressure-induced acoustic velocity reductions appear to be a common characteristic of amorphous phases due to changes in the degree of polymerization.[25-27] The drops of V_P and V_S for the aforementioned amorphous phases are approximately 12% and 18% compared with their crystalline phases, respectively. Interestingly, the velocity reduction from crystalline aragonite to amorphous $CaCO_3$ reaches about 19–42% above 3.5 GPa. At a pressure around 3.6 (1) GPa, the V_P dramatically decreases from 6.20 (7) to 5.01 (6) km s^{-1} at 1,073 K and then to 4.63 (5) km s^{-1} at 1,373 K, while the V_S unexpectedly drops from 3.19(4) to 1.39 (3) km s^{-1} at temperatures above 1,073 K. The intermediate V_P is caused by partial amorphization of aragonite, which can also be observed at1073–1173 K and higher pressures. Moreover, at the maximum pressure of 5.2 (1) GPa in this study, the acoustic velocities greatly reduce from 6.25(8) to 4.19(5) km s^{-1} for the V_P and from 3.19 (4) to 1.54 (2) km s^{-1} for the V_S, respectively, when the aragonite-form $CaCO_3$ fully transforms to the amorphous phase. The minimum V_P value of $CaCO_3$ was 4.13 (5) km s^{-1} at 1,273–1,373 K and 4.0 (1)–5.5 (1) GPa (Figure 2). Compared to the V_P, the V_S is less sensitive to temperature and varies within a relatively narrow range of 1.23 (1)–1.76 (2) km s^{-1} at 1,173–1,373 K and 3.5 (1)–5.2 (1) GPa. Compared to aragonite, the velocity reductions of the amorphous $CaCO_3$ are as high as 35% and 52% for the V_P and V_S, respectively.

DISCUSSIONS

$CaCO_3$ is stable in the cratonic lithosphere according to melting experiments of carbonated peridotite and eclogite below 5 GPa,[28,29] and the Ca/(Ca+Mg) value of quenched carbonate melts approaches 0.96–0.99 as the pressure decreases because of the reaction between dolomitic parental melts and clinopyroxene.[30,31] Consequently, most of the carbonates observed in xenoliths originated from depths of 30–60 km are near the $CaCO_3$ endmember.[4] Alternatively, the $CaCO_3$-rich carbonatites in the Earth's crust could originate from the recycled sediment-bearing oceanic crust.[31,32] $CaCO_3$ is a crystallized phase over large composition and temperature ranges in the ascending carbonatitic melt,[33] and it would be stable under the *P-T* conditions of the cratonic lithosphere. As a matter of fact, $CaCO_3$ in the aragonite form has been proposed to account for seismic anomalies observed in MLDs,[4,11] although the amount of aragonite needed is much higher than the suggested factions of carbonates in the lithosphere.[20]

The acoustic velocities of the amorphous $CaCO_3$ are far below those of the major upper mantle minerals. Clinopyroxenes, olivine, garnet, pyrolite, and mid-ocean ridge basalts exhibit V_P values of about 8.4, 8.5, 9.5, 8.5, and 8.0 km s^{-1}, respectively, and V_S values of about 4.7, 4.8, 5.2, 4.8, and 4.3 km s^{-1}, respectively, under *P-T* conditions similar to this study.[34-40] In comparison, the acoustic velocities of amorphous $CaCO_3$ are 47–56% for the V_P and 65–71% for the V_S lower than those of the common upper mantle components. Even for aragonite, its acoustic velocities are 8–35% lower for the V_P and 8–38% lower for the V_S, respectively. The $CaCO_3$ likely possesses the lowest seismic velocities among all the common minerals and solid aggregates in the Earth's upper mantle. Both the crystalline-amorphization transition and pressure-induced velocity shrink above 3 GPa in $CaCO_3$ could induce low seismic velocity anomalies even if a small amount of $CaCO_3$ is present. The solidified $CaCO_3$ from melts would distribute in the interstitial sites of the silicate matrix according to both high *P-T* experiments[29,41] and xenoliths,[42] forming suitable phase equilibrium aggregates for seismic velocity averaging.

Pyrolite represents the composition of the Earth's ambient upper mantle.[43] Here, we evaluate the effect of $CaCO_3$ on low seismic velocity anomalies by incorporating 2 vol.% $CaCO_3$ in the pyrolite. The calculated seismic velocities are plotted in Figure 3 and Tables S1–S3. The shaded regions in Figure 3 are bounded by the Voigt and Reuss bounds,[44] which denote the upper and lower limits of the seismic velocities, respectively. $CaCO_3$ phases, including the aragonite and amorphous $CaCO_3$ phases, are rheologically and elastically weaker than the co-existing mantle silicates (e.g., olivine, pyroxene, and garnet).[34-40] Thus, the amorphous $CaCO_3$ phase is likely to be strongly deformed, and the mineral matrix in these multi-phase aggregates cannot completely obey either the constant strain assumption for Voigt bound or the constant stress assumption for the Reuss bound. The Hill average, on the other hand, is likely to overestimate the elastic properties of this type of multi-phase rock matrix.[45] The realistic elastic properties of pyrolite + 2.0 vol.% $CaCO_3$ would lie in between the Hill average and the lower Reuss bound. Below 3 GPa and 1,073 K, the aragonite-form $CaCO_3$ is stable and the incorporation of 2.0 vol.% aragonite can only lower the seismic velocity of pyrolite by ~0.5%. However, at higher *P-T* conditions (>3.5 GPa and >1,073 K), after aragonite transforms into the amorphous phase, the velocities of the $CaCO_3$-bearing pyrolite could be significantly decreased. At a depth of ~100 km, the seismic velocities (V_P and V_S) of pyrolite + 2.0 vol.% amorphous $CaCO_3$ are 3.3–5.6% and 5.3–10.3% smaller than those of pyrolite, respectively. If the

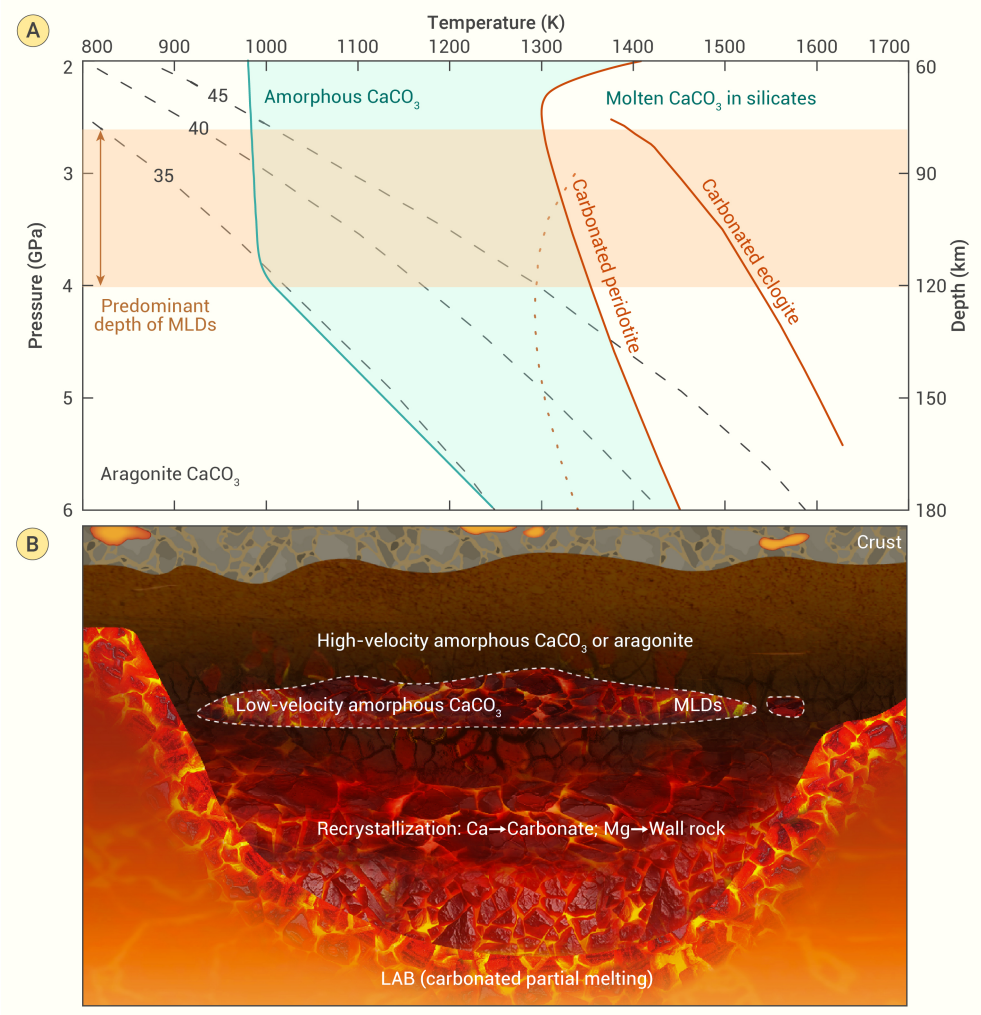

Figure 4. The stability field of amorphous $CaCO_3$ constrained by its phase diagram,[21] craton geotherms (surface heat fluxes of 35, 40, and 45 mW/m^2),[46] and the solidi of carbonated eclogites[41] and peridotite[29] (up) and the schematic of $CaCO_3$-originated seismic abnormalities in the cratonic lithosphere (down) The red dotted curve represents the solidus of carbonated eclogite (Fe-Mg-Ca-Na-K carbonates) from Dasgupta et al..[47] The solidus of carbonated eclogite is significantly affected by the Ca# and Na# in the system. When the carbonate phase is $CaCO_3$, carbonated eclogite melts at much higher temperatures[41].

geotherm is high enough to keep $CaCO_3$ in the amorphous phase at a pressure as low as 2 GPa, the pressure-induced velocity reduction in the amorphous $CaCO_3$ would play the same role as the crystalline-amorphization transition in producing the low seismic velocity anomalies. Thus, a very small amount (e.g., 2.0 vol.%) of $CaCO_3$ can significantly reduce the seismic velocities of pyrolite along the geotherm of the cratonic lithosphere.

$CaCO_3$ is the major carbonate phase stable at the depths of MLDs (Figure 4), which could be distributed in the interstitials of the grains of craton chemical compositions (peridotite, eclogite, and pyroxenites).[28] The analysis of xenoliths indeed shows the presence of $CaCO_3$ at a depth below 40-60 km.[4] As the molten carbonates percolate from the lithosphere-asthenosphere boundary (LAB) or the LAB retreats to greater depths because of the cooling of the Earth, carbonates would crystallize out. Although the primary melts contain significant magnesium (Mg), it would be consumed by the mantle wall rock during ascending upward and the carbonates will be enriched in $CaCO_3$. This has been well confirmed by laboratory experiments and the $CaCO_3$ content in carbonates reaches a maximum around 3–5 GPa.[28] On the other hand, although the solidi of the carbonated peridotite or eclogite are in debated, they are much higher than the geotherms at the MLDs,[28] assuring the solid state of $CaCO_3$ under the explored *P-T* conditions. Over geological time, $CaCO_3$ could accumulate at depths less than 150 km. According to the phase diagram of $CaCO_3$ and the *P-T* conditions of the cratonic lithosphere, the initial solidified $CaCO_3$ would be in the amorphous phase. At depths shallower than ~120 km, the seismic velocities of amorphous $CaCO_3$ are far below those of the main craton minerals and its crystalline phase. As $CaCO_3$ migrates upward, it may transform to the high-velocity aragonite along a cold geotherm or to the high-velocity amorphous $CaCO_3$ at depths shallower than ~80 km along a warm/hot geotherm. Then a seismic velocity discontinuity would be present at depths of 80–120 km due to the crystalline-amorphization transition in $CaCO_3$ and/or the pressure-induced velocity reduction of the amorphous $CaCO_3$. Another potential origin of MLDs is vertical stacking from plume interaction or oceanic subduction. The $CaCO_3$ precipitated from plumes or retained in the oceanic subducted crust would play the same role as that crystallized from ascending carbonates from the LAB in the formation of MLDs. Therefore, the observed 2–10% reduction in the V_S of the MLDs[3-9] would be readily explained by the presence of as low as 2 vol.% $CaCO_3$, which is less than the estimated amount of carbonates in the carbon-rich regions in the lithosphere.[20]

The enrichment and thermodynamic stabilization of the metasomatic $CaCO_3$ in the cratonic lithosphere make it a viable and compelling mechanism to account for the formation of observed MLDs over other explanations. In addition, this mechanism could avoid constraining the $CaCO_3$ in a confined depth range. Even if $CaCO_3$ distributes homogeneously from the surface to a depth of ~150 km, the crystalline-amorphization transition or pressure-induced velocity reduction could guarantee a seismic velocity discontinuity at depths of 80–120 km. This also meets the constraints of global resetting of the age in these regions,[19] as well as magnetotelluric observations.[17,18]

CONCLUSIONS

We measured the acoustic velocities of amorphous $CaCO_3$ up to 5.5 GPa and 1,373 K. Large velocity reductions are observed for both V_P and V_S across the aragonite to temperature-induced amorphous phase transition above ~3 GPa and in the amorphous phase around 3 GPa, which are up to 35% and 52%, respectively. These two distinct features of $CaCO_3$ make it a viable candidate mechanism for the formation of the MLDs in the cratonic lithosphere. The incorporation of ~2 vol.% amorphous $CaCO_3$ could cause the observed 2–10% reduction in seismic velocities in MLDs.

REFERENCES

1. Griffin, W., O'reilly, S.Y., Afonso, J.C., et al. (2009). The composition and evolution of lithospheric mantle: A re-evaluation and its tectonic implications. J. Petrol. **50**: 1185–1204. DOI: 10.1093/petrology/egn033.
2. O'Reilly, S.Y., Griffin, W.L., Djomani, Y.H.P., et al. (2001). Are lithospheres forever? Tracking changes in subcontinental lithospheric mantle through time. GSA today **11**: 4–10. DOI: 10.1130/1052-5173(2001)011<0004:ALFTCI>2.0.CO;2..
3. Selway, K., Ford, H., and Kelemen, P. (2015). The seismic mid-lithosphere discontinuity. Earth Planet. Sci. Lett. **414**: 45–57. DOI: 10.1016/j.epsl.2014.12.029.
4. Rader, E., Emry, E., Schmerr, N., et al. (2015). Characterization and petrological constraints of the midlithospheric discontinuity. Geochem. Geophys, Geosyst. **16**: 3484–3504. DOI: 10.1002/2015GC005943.
5. Karato, S.i. and Park, J. (2018). On the origin of the upper mantle seismic discontinuities. Lithosph. discont. Lithospheric Discontinuities, Huaiyu Yuan and Barbara Romanowicz. pp.5-34. DOI: 10.1002/9781119249740.ch1.
6. Thybo, H. (2006). The heterogeneous upper mantle low velocity zone. Tectonophysics **416**: 53–79. DOI: 10.1016/j.tecto.2005.11.021.
7. Ford, H.A., Fischer, K.M., Abt, D.L., et al. (2010). The lithosphere–asthenosphere boundary and cratonic lithospheric layering beneath Australia from Sp wave imaging. Earth Planet. Sci. Lett. **300**: 299–310. DOI: 10.1016/j.epsl.2010.10.007.

8. Foster, K., Dueker, K., Schmandt, B., et al. (2014). A sharp cratonic lithosphere–asthenosphere boundary beneath the American Midwest and its relation to mantle flow. Earth Planet. Sci. Lett. **402**: 82–89. DOI: 10.1016/j.epsl.2013.11.018.
9. Wirth, E.A. and Long, M.D. (2014). A contrast in anisotropy across mid-lithospheric discontinuities beneath the central United States —A relic of craton formation. Geology **42**: 851–854. DOI: 10.1130/G35804.1.
10. Fu, H.Y., Li, Z.H., and Chen, L. (2022). Continental mid - lithosphere discontinuity: A water collector during craton evolution. Geophys. Res. Lett. **49**: e2022GL101569. DOI: 10.1029/2022GL101569.
11. Eeken, T., Goes, S., Pedersen, H.A., et al. (2018). Seismic evidence for depth-dependent metasomatism in cratons. Earth Planet. Sci. Lett. **491**: 148–159. DOI: 10.1016/j.epsl.2018.03.018.
12. Matsukage, K.N., Nishihara, Y., and Karato, S.i. (2005). Seismological signature of chemical differentiation of Earth's upper mantle. J. Geophys. Res.-Sol. Ea. **110**: B12305. DOI: 10.1029/2004JB003504.
13. Aulbach, S., Massuyeau, M., and Gaillard, F. (2017). Origins of cratonic mantle discontinuities: A view from petrology, geochemistry and thermodynamic models. Lithos **268**: 364–382. DOI: 10.1016/j.lithos.2016.11.004.
14. Saha, S., Dasgupta, R., and Tsuno, K. (2018). High pressure phase relations of a depleted peridotite fluxed by CO_2 - H_2O - bearing siliceous melts and the origin of mid - lithospheric discontinuity. Geochem. Geophys, Geosyst. **19**: 595–620. DOI: 10.1002/2017GC007233.
15. Zhou, W.Y., Hao, M., Zhang, D., et al. (2024). High P - T sound velocities of amphiboles: Implications for low - velocity anomalies in metasomatized upper mantle. Geophys. Res. Lett. **51**: e2023GL106583. DOI: 10.1029/2023GL106583.
16. Massuyeau, M., Gardés, E., Morizet, Y., et al. (2015). A model for the activity of silica along the carbonatite–kimberlite–mellilitite–basanite melt compositional joint. Chem. Geol. **418**: 206–216. DOI: 10.1016/j.chemgeo.2015.07.025.
17. Peng, Y., Manthilake, G., and Mookherjee, M. (2022). Electrical conductivity of metasomatized lithology in subcontinental lithosphere. Am. Mineral. J. Earth Planet. Mater. **107**: 413–420. DOI: 10.2138/am-2021-7942.
18. Hu, X., Lin, W., Yang, W., et al. (2020). A review on developments in the electrical structure of craton lithosphere. Sci. China Earth Sci. **63**: 1661–1677. DOI: 10.1007/s11430-019-9653-2.
19. Carlson, R.W., Pearson, D.G., and James, D.E. (2005). Physical, chemical, and chronological characteristics of continental mantle. Rev. Geophys. **43**: RG1001. DOI: 10.1029/2004RG000156.
20. Foley, S.F. and Fischer, T.P. (2017). An essential role for continental rifts and lithosphere in the deep carbon cycle. Nat. Geosci. **10**: 897–902. DOI: 10.1038/s41561-017-0002-7.
21. Hou, M., Zhang, Q., Tao, R., et al. (2019). Temperature-induced amorphization in $CaCO_3$ at high pressure and implications for recycled $CaCO_3$ in subduction zones. Nat. Commun. **10**: 1963. DOI: 10.1038/s41467-019-09742-5.
22. Kono, Y., Park, C., Kenney-Benson, C., et al. (2014). Toward comprehensive studies of liquids at high pressures and high temperatures: Combined structure, elastic wave velocity, and viscosity measurements in the Paris–Edinburgh cell. Phys. Earth Planet. Inter. **228**: 269–280. DOI: 10.1016/j.pepi.2013.09.006.
23. Suito, K., Namba, J., Horikawa, T., et al. (2001). Phase relations of $CaCO_3$ at high pressure and high temperature. Am. Mineral. **86**: 997–1002. DOI: 10.2138/am-2001-8-906.
24. Ahrens, T.J. and Katz, S. (1963). Ultrasonic observation of the calcite - aragonite transition. J. Geophys. Res.-Sol. Ea. **68**: 529–537. DOI: 10.1029/JZ068i002p00529.
25. Liu, J. and Lin, J.F. (2014). Abnormal acoustic wave velocities in basaltic and (Fe, Al) - bearing silicate glasses at high pressures. Geophys. Res. Lett. **41**: 8832–8839. DOI: 10.1002/2014GL062053.
26. Zha, C.-S., Hemley, R.J., Mao, H.-k., et al. (1994). Acoustic velocities and refractive index of SiO_2 glass to 57.5 GPa by Brillouin scattering. Phys. Rev. B **50**:13105. DOI: 10.1103/PhysRevB.50.13105.
27. Sanchez-Valle, C. and Bass, J.D. (2010). Elasticity and pressure-induced structural changes in vitreous $MgSiO_3$-enstatite to lower mantle pressures. Earth Planet. Sci. Lett. **295**: 523–530. DOI: 10.1016/j.epsl.2010.04.034.
28. Hammouda, T. and Keshav, S. (2015). Melting in the mantle in the presence of carbon: Review of experiments and discussion on the origin of carbonatites. Chem. Geol. **418**: 171–188. DOI: 10.1016/j.chemgeo.2015.05.018.
29. Dasgupta, R., Mallik, A., Tsuno, K., et al. (2013). Carbon-dioxide-rich silicate melt in the Earth's upper mantle. Nature **493**: 211–215. DOI: 10.1038/nature11731.
30. Woolley, A. and Bailey, D. (2012). The crucial role of lithospheric structure in the generation and release of carbonatites: geological evidence. Mineral. Mag. **76**: 259–270. DOI: 10.1180/minmag.2012.076.2.02.
31. Hammouda, T., Chantel, J., Manthilake, G., et al. (2014). Hot mantle geotherms stabilize calcic carbonatite magmas up to the surface. Geology **42**: 911–914. DOI: 10.1130/G35778.1.
32. Yaxley, G.M., Kjarsgaard, B.A., and Jaques, A.L. (2021). Evolution of carbonatite magmas in the upper mantle and crust. Elements **17**: 315–320. DOI: 10.2138/gselements.17.5.315.
33. Weidendorfer, D., Schmidt, M.W., and Mattsson, H.B. (2017). A common origin of carbonatite magmas. Geology **45**: 507–510. DOI: 10.1130/G38801.1.
34. Wang, X., Chen, T., Zou, Y., et al. (2015). Elastic wave velocities of peridotite KLB - 1 at mantle pressures and implications for mantle velocity modeling. Geophys. Res. Lett. **42**: 3289–3297. DOI: 10.1002/2015GL063436.
35. Weidner, D.J., Li, L., Whitaker, M.L., et al. (2018). Ultrasonic acoustic velocities during partial melting of a mantle peridotite KLB - 1. J. Geophys. Res.-Sol. Ea. **123**: 1252–1261. DOI: 10.1002/2017JB014753.
36. Xu, W., Lithgow-Bertelloni, C., Stixrude, L., et al. (2008). The effect of bulk composition and temperature on mantle seismic structure. Earth Planet. Sci. Lett. **275**: 70–79. DOI: 10.1016/j.epsl.2008.08.012.
37. Kono, Y., Irifune, T., Ohfuji, H., et al. (2012). Sound velocities of MORB and absence of a basaltic layer in the mantle transition region. Geophys. Res. Lett. **39**. DOI: 10.1029/2012GL054009.
38. Gwanmesia, G.D., Wang, L., Heady, A., et al. (2014). Elasticity and sound velocities of polycrystalline grossular garnet ($Ca_3Al_2Si_3O_{12}$) at simultaneous high pressures and high temperatures. Phys. Earth Planet. Inter. **228**: 80–87. DOI: 10.1016/j.pepi.2013.09.010.
39. Li, B. and Neuville, D.R. (2010). Elasticity of diopside to 8 GPa and 1073 K and implications for the upper mantle. Phys. Earth Planet. Inter. **183**: 398–403. DOI: 10.1016/j.pepi.2010.08.009.
40. Hao, M., Zhang, J.S., Pierotti, C.E., et al. (2019). High - Pressure single - crystal elasticity and thermal equation of state of omphacite and their implications for the seismic properties of eclogite in the earth's interior. J. Geophys. Res.-Sol. Ea. **124**: 2368–2377. DOI: 10.1029/2018JB016964.
41. Yaxley, G.M., Brey, G.P., and Petrology (2004). Phase relations of carbonate-bearing eclogite assemblages from 2.5 to 5.5 GPa: Implications for petrogenesis of carbonatites. Contrib. Mineral. **146**: 606-619. DOI: 10.1016/j.epsl.2008.08.012.
42. Soltys, A., Giuliani, A., Phillips, D., et al. (2016). In-situ assimilation of mantle minerals by kimberlitic magmas—Direct evidence from a garnet wehrlite xenolith entrained in the Bultfontein kimberlite (Kimberley, South Africa). Lithos **256**: 182–196. DOI: 10.1016/j.lithos.2016.04.011.
43. Ringwood, A.E. (1991). Phase transformations and their bearing on the constitution and dynamics of the mantle. Geochim. Cosmochim. Acta **55**: 2083–2110. DOI: 10.1016/0016-7037(91)90090-R.
44. Hill, R. (1952). The elastic behaviour of a crystalline aggregate. Proc. Phys. Soc.-Sec. A **65**: 349. DOI: 10.1088/0370-1298/65/5/307.
45. Watanabe, T., Shirasugi, Y., and Michibayashi, K. (2014). A new method for calculating seismic velocities in rocks containing strongly dimensionally anisotropic mineral grains and its application to antigorite-bearing serpentinite mylonites. Earth Planet. Sci. Lett. **391**: 24–35. DOI: 10.1016/j.epsl.2014.01.025.
46. Pollack, H.N., Hurter, S.J., and Johnson, J.R. (1993). Heat flow from the Earth's interior: Analysis of the global data set. Rev. Geophys. **31**: 267–280. DOI: 10.1029/93RG01249.
47. Dasgupta, R., Hirschmann, M.M., and Withers, A.C. (2004). Deep global cycling of carbon constrained by the solidus of anhydrous, carbonated eclogite under upper mantle conditions. Earth Planet. Sci. Lett. **227**: 73–85. DOI: 10.1016/j.epsl.2004.08.004.

FUNDING AND ACKNOWLEDGMENTS

The authors would like to thank Dr. Ruijia Wang for constructive discussion about the implications. This work was supported by NSFC-42394114, NSFC-42192535, and NSFC-R22R6402 (M.H.), NSF Grant EAR-2243184 (J.S.Z.), and the National Key Research and Development Program of China (Grant No. 2023YFF0804100) (J.L.). The experiments were performed at HPCAT (Sector 16), Advanced Photon Source (APS), Argonne National Laboratory. HPCAT operation is supported by the DOE-NNSA under Award No. DE-NA0001974, with partial instrumentation funding from the NSF. The Advanced Photon Source is a U.S. Department of Energy (DOE) Office of Science User Facility operated for the DOE Office of Science by Argonne National Laboratory under Contract No. DE-AC02-06CH11357. The founders had no role in study design, data collection and analysis, decision to publish, or preparation of the manuscript.

AUTHOR CONTRIBUTIONS

M.H., J.L., and J.Z. designed the study. M.H., X.S., M.H., W.Z., X.C. and R.H. conducted the experiments. M.H. and M.H. analyzed the experimental data. M.H., J.L., and J.Z. wrote the paper. All the authors contributed to and approved the manuscript.

DECLARATION OF INTERESTS

The authors declare no competing interests.

DATA AND CODE AVAILABILITY

Data are available from the corresponding author upon reasonable request.

SUPPLEMENTAL INFORMATION

It can be found online at https://doi.org/10.59717/j.xinn-geo.2024.100098.

LEAD CONTACT WEBSITE

JinZhang:https://artsci.tamu.edu/geology-geophysics/contact/profiles/jin-zhang.html

Jin Liu: https://scholar.google.com/citations?hl=en&user=IbybMOYAAAAJ